# Spectral Effects of Discrete-Time Amplitude Levels in Digital-Intensive Wideband Radio Transmitters

Mikko Martelius, Kari Stadius, Jerry Lemberg,
Enrico Roverato, Marko Kosunen, and Jussi Ryynänen
Department of Electronics and Nanoengineering, Aalto University
Espoo, Finland
mikko.martelius@aalto.fi

Lauri Anttila and Mikko Valkama
Department of Electronics
and Communications Engineering,
Tampere University of Technology
Tampere, Finland

***Abstract*—This paper examines one source of spectral degradation in polar and multilevel outphasing transmitters. The degradation is caused by the amplitude signal appearing at the transmitter output as a baseband component, in addition to the desired RF signal. This baseband component contains sampling images and quantization noise across the spectrum. Thus, it adds noise at the signal band where it cannot be filtered and limits the achievable ACLR, particularly in wideband LTE and 5G systems. We analyze the origin of this phenomenon and related effects of system and signal parameters, and propose three design solutions for eliminating or alleviating the problem. Our analysis and simulations demonstrate that using a voltage-subtracting power combiner cancels the described degradation, potentially leading to significant improvement in spectral performance.**

## I. Introduction

The development of modern wireless systems has led to strict requirements of transmitter bandwidth and linearity. Meanwhile, the goal of maximizing power efficiency while applying digital-intensive circuit solutions has increased research interest in transmitter architectures that enable both phase and amplitude modulation with efficient but nonlinear switch-mode power amplifiers (PA). Among such transmitters, the optimal back-off power efficiency is typically achieved by architectures that utilize constant-envelope phase-modulated signals and a separate discrete-level amplitude signal. Specifically, this category includes polar [1]–[7] and multilevel outphasing transmitters [8]–[13].

Besides potential for high efficiency and digital-intensive implementation, the described transmitter architectures also feature unique challenges. One of them, as observed in this paper, is that the amplitude signal may appear in the output not only in the form of RF-signal modulation but also as an undesired baseband component. Due to the effects of sampling and quantization, this component produces additional noise at a wide range of frequencies, including the signal band where it cannot be filtered. The use of amplitude levels can thus degrade the adjacent channel leakage ratio (ACLR), particularly in wideband LTE and 5G systems. Consequently, it is crucial to ensure that the transmitter cancels the detrimental baseband signal component in order to optimize its spectral performance.

In order to provide essential insight into the described aspect of transmitter performance, this paper presents comprehensive analysis and simulations of the phenomenon. Furthermore, we examine the arising implications on system-level design choices. Of our proposed solutions, using a voltage-subtracting power combiner is typically the best way to eliminate the undesired signal component. Although such combiners are commonly used, this particular argument for their superiority is previously unreported.

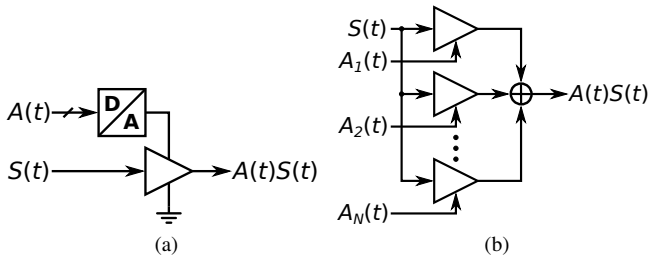


Fig. 1. Amplitude modulation methods: (a) supply modulation; (b) parallel PA units and power combiner.

The rest of this paper is organized as follows: Section II presents an overview of the discussed phenomenon and its origin. Section III contains detailed analysis focusing on multilevel outphasing, with simulations demonstrating the effects of signal bandwidth and amplitude resolution. Three design solutions to the described problem are proposed in Section IV, and Section V concludes the paper.

## II. Overview of the Phenomenon

This paper relates to transmitters in which PA inputs are driven by phase-modulated rail-to-rail signals, and the output amplitude is modulated by a separate discrete-level amplitude signal $A(t)$. This amplitude modulation can be realized by different methods, one of which is modulating the PA supply voltage [9], as shown in Fig. 1(a). Another method, illustrated by Fig. 1(b), is altering the number of active PA units with amplitude bits $A_i(t)$, so that $\sum_{i=1}^{N} A_i(t) = A(t)$ [10], [11]. In both cases, the output signal is $A(t)S(t)$, where $S(t)$ is the phase-modulated input signal. Therefore, in the context of the following analysis, there is effectively no difference between these methods. Either system in Fig. 1 is hereafter presented as a single PA with $A(t)$ as its amplitude-control signal.

Fig. 2 shows the block diagrams of power amplification and output-signal construction in polar and multilevel outphasing transmitters that combine all signals by addition. In polar transmitters, the PA input signals are the constant-envelope phase-modulated signal $S_{in}(t)$ and the amplitude signal $A(t)$.

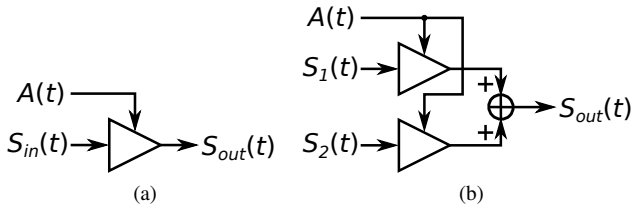


Fig. 2. Block diagrams of power amplification in (a) polar and (b) multilevel outphasing transmitters.

When the supply voltage is normalized to one, $S_{in}(t)$ is a square wave between zero and one, modulated by delaying the entire waveform. Derived from the Fourier series of a square wave, the signal can be expressed as

$$S_{in}(t) = \frac{1}{2} + \frac{2}{\pi}\sum_{k=1}^{\infty}\frac{\sin\left[(2k-1)(\omega_c t + \phi(t))\right]}{2k-1}, \quad (1)$$

where $\omega_c$ is the carrier frequency and $\phi(t)$ is the modulated phase. By multiplying $S_{in}(t)$ by $A(t)$, we obtain

$$S_{out}(t) = \frac{A(t)}{2} + \frac{2A(t)}{\pi}\sum_{k=1}^{\infty}\frac{\sin\left[(2k-1)(\omega_c t + \phi(t))\right]}{2k-1}. \quad (2)$$

Multilevel outphasing transmitters can be analyzed in a similar manner. Both $S_1(t)$ and $S_2(t)$ are phase-modulated square waves, and they can be written as

$$S_{1,2}(t) = \frac{1}{2} + \frac{2}{\pi}\sum_{k=1}^{\infty}\frac{\sin\left[(2k-1)(\omega_c t + \Phi_{1,2}(t))\right]}{2k-1}, \quad (3)$$

where $\Phi_1(t) = \phi(t) + \theta(t)$ and $\Phi_2(t) = \phi(t) - \theta(t)$, $\phi(t)$ is the phase modulation of the output signal, and $\theta(t)$ is the outphasing angle. $S_1(t)$ and $S_2(t)$ are both multiplied by $A(t)$ and added, leading to the output signal

$$S_{out}(t) = A(t) + \frac{4A(t)}{\pi}\sum_{k=1}^{\infty}\frac{\cos\left[(2k-1)\theta(t)\right]\sin\left[(2k-1)(\omega_c t + \phi(t))\right]}{2k-1}. \quad (4)$$

Equations (2) and (4) reveal the central observation of this paper: in both polar and multilevel outphasing transmitters, the output signal includes the baseband amplitude signal $A(t)$ with a constant multiplier. This is because the output signal always alters between zero and a value defined by the amplitude level, which leads to an asymmetric signal. Another interpretation is that $A(t)$ also modulates the non-zero DC level of the rail-to-rail input signals in addition to the RF components. This phenomenon is illustrated in time domain by Fig. 3. For the purposes of subsequent analysis, we separate the output signals of (2) and (4) into two components. We will refer to the first term—$kA(t)$—as the baseband (BB) component, and the second term—a sum of high-frequency signals multiplied by $A(t)$—will be called the RF component.

The amplitude signal is sampled and held at a rate of $f_s$, and therefore the BB component includes sampling images at $f_s$ and its harmonics. When the carrier frequency $f_c$ is equal to $f_s$ or its multiple, one of the images appears around the signal

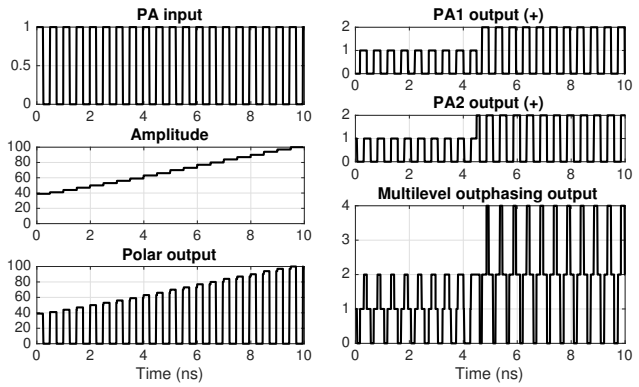


Fig. 3. Time-domain (a) polar and (b) multilevel outphasing signals.

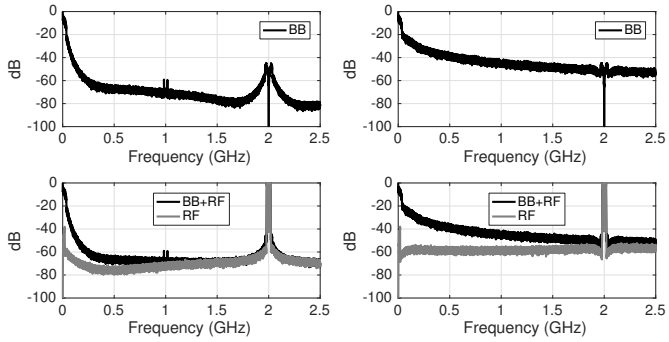


Fig. 4. Spectra of output-signal components with (a) polar and (b) multilevel outphasing transmitters using 40-MHz aggregated LTE signals.

band, where the additional noise limits the ACLR. Moreover, the BB component contains quantization noise throughout the spectrum. These spectral effects are shown in Fig. 4, which depicts the output-signal components of a 40-MHz aggregated LTE signal with both transmitter architectures, when $f_c = f_s = 2$ GHz. All shown results have been simulated in Matlab with a model of a delay-line-based phase modulator [14], unless otherwise mentioned. This choice does not affect the essential observations, because the amplitude signal is independent of the phase-modulation method.

Although DC-block capacitors and resonators are able to filter the low and high-frequency parts of the BB component, they cannot remove the additional noise near the signal band. Therefore, it is necessary to design the transmitter so that it cancels the BB component at the output. Potential ways of achieving this will be discussed in Section IV.

## III. Analysis with Multilevel Outphasing

This section analyzes the effects of the previously defined BB component in detail, focusing entirely on multilevel outphasing. This choice was made because the spectral performance of polar transmitters depends crucially on fine amplitude resolution, whereas in multilevel outphasing, amplitude levels mainly exist to improve the power efficiency. Thus, the spectral effects of amplitude resolution in multilevel outphasing are more predominantly related to the BB component.

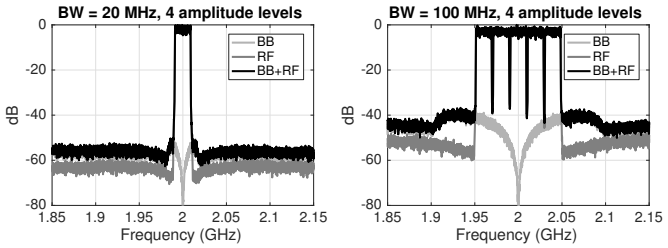


Fig. 5. Spectra of the output-signal components with different bandwidths.

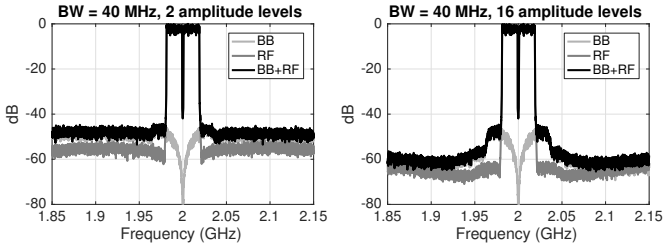


Fig. 6. Spectra of the output-signal components with amplitude resolutions.

Fig. 5 depicts simulated spectra of 20-MHz and 100-MHz LTE signals where $f_c = f_s = 2$ GHz, both with 4 amplitude levels. The BB and RF components are shown along with the complete output signal, demonstrating that the BB component dominates the noise outside the signal band. The sampling image appears as mirror images on both sides of the sample frequency, covering in total twice the signal bandwidth. The BB component has a zero-order-hold charasteristic corresponding to a sinc frequency response, whose attenuation increases as the frequency approaches $f_s$. With sufficiently narrow bandwidths, the image is thus attenuated enough to become insignificant compared to other sources of noise. Wideband images, however, remain much stronger and are likely to dominate the noise, setting a limit to the ACLR.

To illustrate the effects of amplitude resolution, Fig. 6 shows the spectra of 40-MHz aggregated LTE signals with 2 and 16 amplitude levels. With 2 levels, the quantization noise of the BB component is dominant enough to render the sampling image at 1.96–2.04 GHz barely noticeable. Increasing the resolution reduces the quantization noise, making the image more visible. However, the noise level near the signal band, which defines the ACLR, is virtually equal in both presented cases. Thus, the amplitude resolution primarily affects the BB-component spectrum further from the signal band.

Table I presents the ACLR results with all simulated combinations of bandwidth, amplitude levels, and inclusion or exclusion of the BB component. These results confirm the observation that the BB component has a more dominant effect with wide bandwidths. In the separated RF component, increasing the amplitude resolution from 2 to 16 levels improves the ACLR by 6.2–7.7 dB, but when the BB component is included, the amplitude resolution only has a significant effect on the ACLR with a 20-MHz bandwidth. In general, eliminating the BB component at the output is shown to produce a considerable ACLR improvement of 7.8–16.7 dB.

TABLE I. SIMULATED ACLR (BB+RF / RF).

| ACLR (dBc) | 2 ampl. levels | 4 ampl. levels | 16 ampl. levels |
|---|---|---|---|
| BW = 20 MHz | -52.1 / -60.1 | -54.3 / -63.4 | -56.2 / -73.3 |
| BW = 40 MHz | -45.2 / -55.0 | -45.9 / -59.2 | -46.4 / -61.6 |
| BW = 100 MHz | -36.8 / -47.8 | -37.1 / -52.7 | -37.3 / -54.0 |

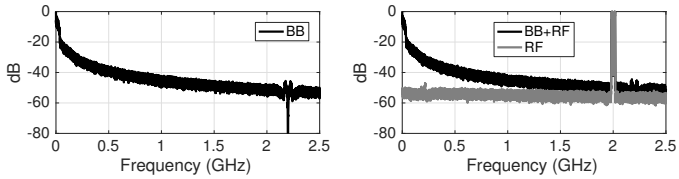


Fig. 7. Spectra of 40-MHz output-signal components with multilevel outphasing, when $f_s \neq f_c$.

## IV. SOLUTIONS

This section presents three design solutions that can either remove the BB component from the output or at least reduce its degrading effects.

### A. Unequal Sample Rate and Carrier Frequency

The ACLR degradation caused by the BB component can be somewhat alleviated by using a sample rate that is not equal to the carrier frequency or any of its integer fractions, thus moving the sampling image away from the signal band. This solution is made possible by the digital interpolating phase modulator (DIPM), which is capable of generating a phase-modulated signal at any carrier frequency within certain limits [13], [15]. Fig. 7 shows an example of this approach, simulated with a Matlab model of the DIPM, in which $f_s = 2.2$ GHz and $f_c = 2$ GHz. This solution is far from perfect, as it does not remove the BB component but only shifts the sampling image to a different frequency. As such, the quantization noise across the spectrum can still degrade the ACLR to a lesser extent.

### B. Voltage Subtraction in Power Combining

The BB component can be entirely canceled at the output by using a power combiner that subtracts one voltage from another instead of adding all voltages. Existing implementations of such combiners are typically based on transformers [10], [16]–[18] or coupled transmission lines [19]–[23].

Fig. 8 depicts block diagrams of polar and multilevel-outphasing power amplification with voltage-subtracting power combiners. In polar transmitters, as seen in Fig. 8(a), this solution leads to a structure with somewhat higher complexity compared to Fig. 2(a). Namely, the system requires a second PA with an inverted input signal and a power combiner that cancels the common-mode BB component at the output. In multilevel outphasing, however, a very similar structure can be used with both types of power combiners, as shown in Fig. 8(b). Here, changing the combiner type does not increase the system complexity, because two different phase-modulated input signals are required in either case. Power-loss differences between combiner types may have a slight effect on efficiency.

With the polar signals shown in Fig. 8(a), the output is

$$S_{out} = A(t)[S_{in}(t) - (1 - S_{in}(t))], \tag{5}$$

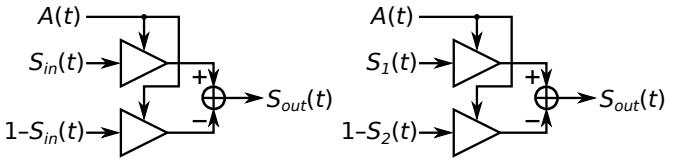


(a) (b)

Fig. 8. Block diagrams of power amplification in (a) polar and (b) multilevel outphasing transmitters with subtracting power combiners.

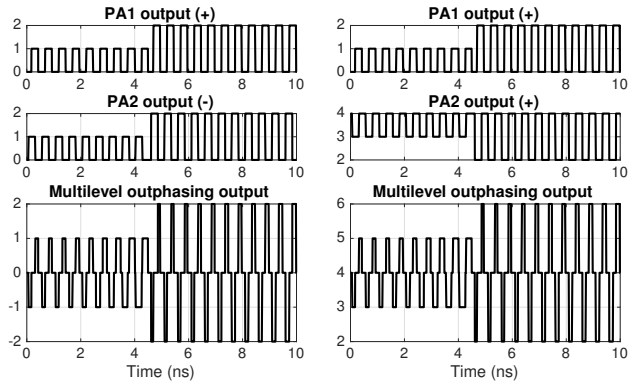


(a) (b)

Fig. 9. Time-domain waveforms with (a) a voltage-subtracting power combiner; (b) baseband-canceling PAs.

and by substituting $S_{in}(t)$ from (1), the result is

$$S_{out}(t) = \frac{4A(t)}{\pi} \sum_{k=1}^{\infty} \frac{\sin\left[(2k-1)(\omega_c t + \phi(t))\right]}{2k-1}. \quad (6)$$

Similarly, with the multilevel outphasing signals in Fig. 8(b),

$$S_{out} = A(t)[S_1(t) - (1 - S_2(t))]. \quad (7)$$

By substituting $S_1(t)$ and $S_2(t)$ from (3), we obtain

$$S_{out}(t) = \frac{4A(t)}{\pi} \sum_{k=1}^{\infty} \frac{\cos\left[(2k-1)\theta(t)\right] \sin\left[(2k-1)(\omega_c t + \phi(t))\right]}{2k-1}. \quad (8)$$

As seen in (6) and (8), the output signal with a voltage-subtracting combiner only contains the RF component depicted in Figs. 5 and 6. Thus, the spectrum is substantially improved, as comparison between BB+RF and RF components reveals. A time-domain example of multilevel-outphasing waveforms with a voltage-subtracting combiner is shown in Fig. 9(a).

### C. Baseband-Canceling PA Design

When using a voltage-adding power combiner, the BB component can be canceled by taking the discussed phenomenon into consideration in PA design, leading to the spectra shown as the RF component in Figs. 5 and 6. This is only possible with class-D PAs capable of holding the maximum output voltage for an arbitrarily long time. Moreover, it requires realizing the amplitude levels by altering the number of active PA units instead of supply modulation.

When the baseband-canceling PA pair is inactive, the output voltage remains low in one PA and high in the other.

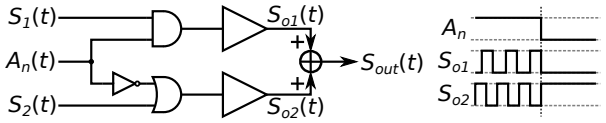


Fig. 10. Conceptual block diagram of a baseband-canceling PA pair.

Consequently, the BB components at PA outputs add up to a DC voltage, which can be removed by a DC-block capacitor. An example of the resulting multilevel-outphasing waveforms is shown in Fig. 9(b). Fig. 10 depicts a block diagram of such a PA pair, where the input signals are combined with different logic gates. In practice, delay mismatches between input signals need to be eliminated by meticulous design of the logic gates or additional delay-compensation elements.

### D. Comparison of the Proposed Solutions

As previously mentioned, moving the sample rate away from the carrier frequency is only a partial solution, as quantization noise of the BB component will nevertheless appear around the signal band. However, this is the only suggested solution that is possible without a power combiner. Thus, despite its flaws, this approach might be the most feasible option in some relatively narrow-band polar transmitters with high amplitude resolution, if area restrictions prevent including the passive components of a power combiner.

Of the two solutions that entirely remove the BB component, voltage subtraction is typically more convenient. This is particularly true in multilevel outphasing transmitters, where it does not increase system complexity or restrict other design choices. In contrast, the baseband-canceling PA structure is only possible with class-D PAs, and it requires careful design in order to avoid timing mismatches between PA units and consequent nonlinearity. Thus, we conclude that in order to optimize the transmitter performance, a voltage-subtracting power combiner should be utilized whenever possible.

## V. Conclusion

In this paper, we have analyzed the spectral effects of the discrete-time amplitude signals used in polar and multilevel outphasing transmitters. We observed that when rail-to-rail input signals are multiplied by an amplitude signal and added, the output contains the amplitude signal as a baseband component in addition to the desired RF signal. Due to sampling images and quantization, this component adds unwanted noise not only near DC but also at the signal band, where it limits the achievable ACLR. As such, considering this phenomenon is an essential aspect of optimizing the spectral performance of digital-intensive transmitters, particularly with the extremely wide bandwidths of future 5G systems. Based on the comparison between our three proposed solutions, we generally recommend using a voltage-subtracting power combiner, which solves the discussed problem by entirely canceling the undesired baseband signal component.


## Acknowledgment

This work is supported by Nokia, the Finnish Funding Agency for Technology and Innovation, and the Academy of Finland.

## REFERENCES


[1] M. R. Elliott *et al.*, "A polar modulator transmitter for GSM/EDGE," *IEEE J. Solid-State Circuits*, vol. 39, no. 12, pp. 2190–2199, Dec 2004.

[2] R. B. Staszewski *et al.*, "All-digital PLL and transmitter for mobile phones," *IEEE J. Solid-State Circuits*, vol. 40, no. 12, pp. 2469–2482, Dec 2005.

[3] J. W. Lai *et al.*, "A 0.27mm$^2$ 13.5dBm 2.4GHz all-digital polar transmitter using 34%-efficiency Class-D DPA in 40nm CMOS," in *2013 IEEE Int. Solid-State Circuits Conf. Dig. Tech. Papers (ISSCC)*, Feb 2013, pp. 342–343.

[4] V. Kopta, R. Thirunarayanan, F. Pengg, E. L. Roux, and C. Enz, "A 2.4-GHz low complexity polar transmitter using dynamic biasing for IEEE 802.15.6," in *2015 IEEE Int. Symp. Circuits and Systems (ISCAS)*, May 2015, pp. 1686–1689.

[5] M. Fulde *et al.*, "A digital multimode polar transmitter supporting 40MHz LTE carrier aggregation in 28nm CMOS," in *2017 IEEE Int. Solid-State Circuits Conf. (ISSCC)*, Feb 2017, pp. 218–219.

[6] P. Madoglio *et al.*, "A 2.4GHz WLAN digital polar transmitter with synthesized digital-to-time converter in 14nm trigate/FinFET technology for IoT and wearable applications," in *2017 IEEE Int. Solid-State Circuits Conf. (ISSCC)*, Feb 2017, pp. 226–227.

[7] Q. Zhu *et al.*, "A digital polar transmitter with DC-DC converter supporting 256-QAM WLAN and 40-MHz LTE-A carrier aggregation," *IEEE J. Solid-State Circuits*, vol. 52, no. 5, pp. 1196–1209, May 2017.

[8] K.-Y. Jheng, Y.-C. Chen, and A.-Y. Wu, "Multilevel LINC system designs for power efficiency enhancement of transmitters," *IEEE J. Sel. Topics Signal Process.*, vol. 3, no. 3, pp. 523–532, June 2009.

[9] P. Godoy, S. Chung, T. Barton, D. Perreault, and J. Dawson, "A 2.4-GHz, 27-dBm asymmetric multilevel outphasing power amplifier in 65-nm CMOS," *IEEE J. Solid-State Circuits*, vol. 47, no. 10, pp. 2372–2384, Oct 2012.

[10] W. Tai *et al.*, "A transformer-combined 31.5 dBm outphasing power amplifier in 45 nm LP CMOS with dynamic power control for back-off power efficiency enhancement," *IEEE J. Solid-State Circuits*, vol. 47, no. 7, pp. 1646–1658, July 2012.

[11] M. Martelius *et al.*, "Class D CMOS power amplifier with on/off logic for a multilevel outphasing transmitter," in *2016 IEEE Int. Symp. Circuits and Systems (ISCAS)*, May 2016, pp. 710–713.

[12] J. Hur *et al.*, "A multilevel class-D CMOS power amplifier for an outphasing transmitter with a nonisolated power combiner," *IEEE Trans. Circuits Syst. II*, vol. 63, no. 7, pp. 618–622, July 2016.

[13] M. Kosunen *et al.*, "A 0.35-to-2.6GHz multilevel outphasing transmitter with a digital interpolating phase modulator enabling up to 400MHz instantaneous bandwidth," in *2017 IEEE Int. Solid-State Circuits Conf. (ISSCC)*, Feb 2017, pp. 224–225.

[14] A. Ravi *et al.*, "A 2.4-GHz 20–40-MHz channel WLAN digital outphasing transmitter utilizing a delay-based wideband phase modulator in 32-nm CMOS," *IEEE J. Solid-State Circuits*, vol. 47, no. 12, pp. 3184–3196, Dec. 2012.

[15] J. Lemberg *et al.*, "Digital interpolating phase modulator for wideband outphasing transmitters," *IEEE Trans. Circuits Syst. I*, vol. 63, no. 5, pp. 705–715, May 2016.

[16] I. Aoki, S. D. Kee, D. B. Rutledge, and A. Hajimiri, "Distributed active transformer—a new power-combining and impedance-transformation technique," *IEEE Trans. Microw. Theory Tech.*, vol. 50, no. 1, pp. 316–331, Jan 2002.

[17] J. Jang, C. Park, H. Kim, and S. Hong, "A CMOS RF power amplifier using an off-chip transmision line transformer with 62% PAE," *IEEE Microw. Wireless Compon. Lett.*, vol. 17, no. 5, pp. 385–387, May 2007.

[18] H. Xu, Y. Palaskas, A. Ravi, M. Sajadieh, M. A. El-Tanani, and K. Soumyanath, "A flip-chip-packaged 25.3 dBm class-D outphasing power amplifier in 32 nm CMOS for WLAN application," *IEEE J. Solid-State Circuits*, vol. 46, no. 7, pp. 1596–1605, July 2011.

[19] M. P. van der Heijden, M. Acar, J. S. Vromans, and D. A. Calvillo-Cortes, "A 19W high-efficiency wide-band CMOS-GaN class-E Chireix RF outphasing power amplifier," in *IEEE MTT-S Int. Microw. Symp.*, June 2011.

[20] A. N. Stameroff, H. H. Ta, A. V. Pham, and R. E. Leoni III, "Wide-bandwidth power-combining and inverse class-F GaN power amplifier at X-band," *IEEE Trans. Microw. Theory Tech.*, vol. 61, no. 3, pp. 1291–1300, March 2013.

[21] H.-C. Park, S. Daneshgar, Z. Griffith, M. Urteaga, B. S. Kim, and M. Rodwell, "Millimeter-wave series power combining using sub-quarter-wavelength baluns," *IEEE J. Solid-State Circuits*, vol. 49, no. 10, pp. 2089–2102, Oct 2014.

[22] H. Jia, B. Chi, L. Kuang, and Z. Wang, "A W-band power amplifier utilizing a miniaturized Marchand balun combiner," *IEEE Trans. Microw. Theory Tech.*, vol. 63, no. 2, pp. 719–725, Feb 2015.

[23] S. Muralidharan, K. Wu, and M. Hella, "A compact low loss single-ended to two-way differential power divider/combiner," *IEEE Microw. Wireless Compon. Lett.*, vol. 25, no. 2, pp. 103–105, Feb 2015.